Ar^+ ion irradiation-induced reorganization of colloidal silica nanoparticles in Langmuir-Blodgett monolayers

S. Lugomer, Z. Zolnai, A.L. Tóth, A. Deák, N. Nagy

PII: S0040-6090(14)01254-1
DOI: doi: 10.1016/j.tsf.2014.11.090
Reference: TSF 33960

To appear in: *Thin Solid Films*

Received date: 10 March 2014
Revised date: 28 November 2014
Accepted date: 28 November 2014

Please cite this article as: S. Lugomer, Z. Zolnai, A.L. Tóth, A. Deák, N. Nagy, Ar^+ ion irradiation-induced reorganization of colloidal silica nanoparticles in Langmuir-Blodgett monolayers, *Thin Solid Films* (2014), doi: 10.1016/j.tsf.2014.11.090

Ar^+ ion irradiation-induced reorganization of colloidal silica nanoparticles in Langmuir-Blodgett monolayers

S. Lugomer[1*], Z. Zolnai[2], A. L. Tóth[2], A. Deák[2] , N. Nagy[2]

[1] «Rudjer Boskovic» Institute, Bijenicka c. 54, 10001 Zagreb, Croatia.

[2] Research Centre for Natural Sciences, Institute of Technical Physics and Materials Science, Hungarian Academy of Sciences, 1121 Budapest, Konkoly Thege M. út 29-33, Hungary.

*****Corresponding author: lugomer@irb.hr

Key words: Nanoparticles, Self-organization, Langmuir-Blodgett layer, ion irradiation

ABSTRACT

The Ar^+ ion irradiation-induced reorganization of Langmuir-Blodgett monolayers of colloidal silica nanoparticles with diameter of 220 nm and 450 nm deposited on silicon substrate is investigated in a wide range of ion fluences. The cluster formation, average cluster size, ion beam-induced charging and discharging of particles, heating effects, the ion beam-induced viscous flow as well as the swelling of the Si substrate as a function of the ion fluence are discussed. Inhomogeneous particle distribution causes strong nonlinear Si swelling inside wide defect-channels between the clusters and linear Si swelling inside narrow channels between the particles. At low ion fluences particle charging and Coulomb repulsion forces govern the particle reorganization process, while at high ion fluences ion beam-induced viscous flow and hydrodynamic forces between the particles and the underlying substrate play major role. Two different types of patterns: smaller compact clusters of few particles and longer chain-like clusters of dozens of particles are observed. The dynamics of the reorganization process in both cases is treated analogous to the dynamics of colloidal suspensions based on the

Tanaka-Araki model. The results of the model are comparable to the experimentally observed cluster characteristics.

1. INTRODUCTION

The nanopatterning of thin films by low- and medium-energy ion irradiation through a Langmuir-Blodgett (LB) monolayer of silica particles (nanomasks) is a widely used technique for electrical and optical applications [1-4]. The nanomasks are densely packed hexagonally ordered systems of silica particles used for the local modification of macroscopic surfaces at the nanoscale. However, the modification is usually associated with complex processes which can affect surface patterning by the change of the particle size and shape, nanomask geometry, as well as of the surface morphology of the substrate.

These phenomena should be understood in order to get full control of the surface nanopatterning process. At low and medium fluence this process depends on the charging of particles and relation between Coulomb and friction forces [5, 6], proximity effects [7, 8] and the swelling of the silicon substrate. At high fluence, discharging and thermal effects like 2D surface

melting, as well as the floating, sputtering and buckling of particles [5, 6, 9, 10] take place. The physical parameters playing crucial role in such effects are ion energy, ion mass, particle size and shape, particle-particle distance and the initial self-organization of particles in the LB monolayer [5, 6]. So far low mass ions like He^+ [11], medium mass ions like Ar^+ or Ga^+ [5, 6], and heavy ions like Xe^+ [12, 13], Xe^{2+} [7, 14] or Xe^{4+}[15] have been used for the irradiation of various materials and study of the above mentioned phenomena.

The ion irradiation of a nanoparticulate mask causes the reorganization of particles with different features of the process for low, medium and high ion fluences [16, 17]. In this paper we show that the reorganization process also depends on the particle size. Also, difference between the reorganization process induced by 30 keV Ga^+ ions from a focused ion beam source (our previous work [6]) and 40 keV Ar^+ ions from a conventional implanter (our present work), is shown. At low fluence, the LB layer becomes the system of “solid particles on the solid substrate”. At higher fluence, surface swelling and irradiation-induced flow take place so that the LB layer becomes the system of “solid particles on the soft surface”, or “soft particles on the soft surface”. We show that relationship between the

dynamics of ion-irradiated particle systems and the dynamics of a colloidal suspension of solid or softened particles can be established since both types of reorganization process can be related to certain types of experimentally observed clusters.

2. EXPERIMENTAL DETAILS

Monolayers of medium and large size silica nanoparticles were prepared using Stöber's method [18] based on controlled hydrolysis of tetraethyl-orthosilicate. The diameters of the medium and large size particles were D = 220 ± 20 nm and D = 450 ± 35 nm, respectively, as it was shown by Field Emission Scanning Electron Microscopy (FESEM) analysis. The LB-film deposition was carried out with a KSV2000 film balance on 25 × 25 mm^2 rectangular (100) oriented p-type (14–27 Ωcm) silicon substrates using vertical deposition method. Detailed description of the LB monolayer preparation is given in refs. [6, 19, 20]. The self-organization of particles in the LB layer changes with increasing the particle size and this "size effect" emerges from the relation between inter-particle and hydrodynamic forces [6]. The inter-particle forces dominate the viscosity at low shear stress in the suspending medium. In contrast, hydrodynamic forces dominate at higher

shear stress showing shear thickening and tendency to anisotropic organization with increasing particle size. The drying process at ambient temperature fixes the silica particles at their position in the LB monolayer [6].

In this work, the irradiation of LB layers was performed with low energy (E = 40 keV) Ar^+ ions in a vacuum chamber at the pressure of about 10^{-4} Pa. Note, in our previous work [6] on 30 keV Ga^+ irradiation, the liquid metal ion source of a LEO Focused Ion Beam System has been applied, while in this work for the Ar^+ ion bombardment experiments a Varian type implanter has been used. Note, the spot size of the Ar^+ ion beam was about 60 mm^2 with a beam current of ~1μA, while for the Ga^+ beam the maximum spot diameter was about 100-200 nm, with a beam current of ~1 nA. Consequently, the local ion flux for Ar^+ was about 10^{13} $cm^{-2}s^{-1}$, i.e., orders of magnitude lower than the value of ~10^{18} $cm^{-2}s^{-1}$ used for Ga^+. In both cases the beam was scanned, however, with somewhat different conditions; i.e., different window areas were scanned with a frequency of 50 Hz for Ga+, and in the frequency range 0.1-1 kHz for Ar+, respectively.

A set of samples has been irradiated with Ar^+ fluences of 0.1, 0.5, 1, 5, and 10 ($\times 10^{16} cm^{-2}$) in the current density range of 0.5 - 2 μA cm^{-2}, with typical input power density range of 0.02 - 0.1 W cm^{-2}.

Besides irradiation-induced charging, heating, and flow processes one has to consider the effects of contamination of the LB layer of silica particles during the reorganization process. Strictly speaking, the contamination may be caused by both the particle preparation process, and by the ion beam irradiation treatment.

The contamination in the preparation process is induced by the tetraethyl orthosilicate hydrolysis, in ethanolic medium in the presence of ammonia [21]. Measurements by various diagnostic techniques discovered the presence of Si, O and C elemental contaminants in the SiO_2 particles, as well as of some hydrogen-carbon compounds [21]. The silica particles of larger diameter have a higher O/Si ratio at their surface, as compared to their cores [21]. The presence of C atoms originates from unhydrolyzed ethoxy groups. The C-compounds found in particle surface-shells and in their cores represent the non-dialyzable non-volatile C-compounds. Their presence on the particle surface was detected by electron energy loss spectroscopy, a technique endowed with single-atom sensitivity. Thus, in principle, the SiO_2 particles formed by the Stöber method always comprise the above contaminants in the amount that is proportional to their size.

The contamination induced by ion beam irradiation basically depends on the presence of residual gas, implantation of the primary ions, and on sputtering. Some residual gas always present when ion irradiation is performed in a vacuum chamber with low pressure conditions. In this case the surface contamination primarily originates from the amount of residual gas (mainly hydrocarbon) molecules deposited to the sample surface by the assistance of the ion beam itself.

The contamination by sputtering becomes particularly intense when the ion flux reaches $10^{16}cm^{-2}$ or more. Ryssel *et al.* [22] performed experiments by As+ ion bombardment of silicon in the fluence range of 10^{12} - 10^{17} cm^{-2} and caused the contamination with Al atoms, The concentration of Al atoms transferred to the silicon wafer during the As+ bombardment process has been measured [22]. It was found that the amount of contaminated Al linearly increases with fluence and reaches saturation at ~ 3 x 10^{13} (Al atoms/cm^2) at the ion fluence of ~ 5 x 10^{15} As+ cm^{-2}. The higher the As+ ion energy the higher the saturation amount of Al contaminated [22].

Therefore, ion beams in the 100 keV energy range cause contamination which linearly depends on the ion fluence up to a threshold value when it turns to saturation.

Considering our experiments, we can state that the contamination of the silica particles by Si, C, and O components is present due to the Stöber formation process [21], but their concentration is larger for 450 nm than for 220 nm diameter. On the other hand, the contamination due to the Ar+ ion beam deposited residual gas molecules is expected to linearly increase with the fluence up to ~ 10^{15} cm^{-2} when reaches saturation. The contamination can affect the reorganization process by influencing the charging of particles, or by causing thermal effects. The influence of charging effects on particle reorganization in the fluence range up to $\leq$ 10^{15} cm^{-2}, i.e., at low contamination levels, is almost negligible. The influence of heating processes on reorganization may, in principle, occur through the change of the timescale of thermalization. However, the steady state temperatures are most probably unaffected by the contaminated layer which may act as a heat transfer layer but not as a heat sink. Thus, the contamination effects are not expected to play significant role in the reorganization of particles.

The self-organization of nanoparticles in the initial LB layers, as well as their reorganization after ion irradiation have been studied by FESEM using the LEO 1540 XB cross-beam system at an operating voltage of 2 kV.

Atomic force microscopy (AFM) analysis has been performed with an Advanced Integrated Scanning Tools for Nano Technology (AIST-NT) type Smart Scanning Probe Microscope 1010 setup operating in tapping mode. The measured AFM data were processed using the Gwyddion software, type 2.26 (publisher: David Necas and Petr Klapetek, Czech Metrology Institute).

3. RESULTS AND DISCUSSION

3.1 Characteristics of initial LB layers of silica nanoparticles

3.1.1 Medium-size particles: D = 220 nm

The SEM micrograph in Fig. 1(a) shows the inhomogeneous LB layer of $D \sim 220$ nm particles with the area number density of $\rho_s \sim 2.1\times10^9 cm^{-2}$. Some regions of the LB layer show selforganization into large quasi-regular 2D crystals with well defined boundaries (defect-channels) between the crystal-grains of ~100–150 nm width and ~ 600–800 nm length. The insets to Fig.1(a) show other regions which comprise zig-zag rhombic clusters, and the chevron-type clusters of three connected hexagons. Such inhomogeneity of particle self-organization results from the interplay of hydrodinamic and short-range repulsive forces [6,23]. The tendency to anisotropic organization

during the formation of LB layer indicates the increase of the short-range repulsive forces, and the decrease of the lubrication hydrodynamic forces with lower shear viscosity – or shear thinning [6,23,24]. The non-Newtonian behavior in a lower density system of medium-size particles causes the short range anisotropy in the nearest pair distribution [6,23].

3.1.2 Large-size particles: D = 450 nm

The SEM micrograph in Fig.1(b) shows the LB layer of $D \sim 450$ nm particles with more regular - almost homogeneous - particle distribution with area number density of $\rho_s \sim 5\times10^8 cm^{-2}$. The insets to Fig.1b show a rhombic cluster (top right) and irregular particle aggregates (bottom right). The self-organization into crystal grains with large grain boundaries reveals the impact of long-range anisotropic organization. This process relates to the appearance of the 2D nanocrystal blocks separated by the long grain-boundaries of about 150–180 nm width. The local particle organization comprises large rhombic blocks with the angles of 60^o and 120^o which contain hexagonally ordered cells. Such self-organization is different from the regular hexagonal order of a closely packed nanoparticulate film. This indicates the increased account of repulsive short-range forces which prevent

particles from getting closer, so that hydrodynamic lubrication forces cannot have important role [23]. A low shear rate generates shear thinning, which for the low particle density causes the long-range anisotropy in the nearest-neighbor distributions and results in the formation of 2D rhombic nanocrystals in the initial LB layer.

3.2 Reorganization of LB layers of silica nanoparticles

3.2.1. *Medium size particles*

The SEM micrograph of the reorganized LB layer of medium-size particles irradiated in the fluence range 1×10^{15}cm^{-2} – 5×10^{15}cm^{-2} shows quasi-regular organization (Fig. 2a(i)). The repulsive Coulomb interaction between the particles causes slight translation of crystal grains as well as breaking of the initial organization into rhombic, trapezoidal and other polygonal grain clusters (Fig. 2a(ii)). At the higher fluence of 10^{16}cm^{-2}, the Coulomb force causes the motion of particles as the «solid particles on the solid substrate» and transformation of the rhombic grains into new cluster types (Fig. 2b(i)) connected into complex polygonal form (Fig. 2b(ii)).

Further increase of the fluence to 5×10^{16}cm^{-2} causes more dramatic LB layer reorganization, as it is shown in Fig. 3:

(i) Breaking of the large grain-clusters into smaller ones of 6 to 8 particles (aggregates).

(ii) Formation of large defect-channels of ~200 nm width between the clusters.

(iii) Motion of particles and even of the whole clusters.

(iv) Strong swelling of the Si single crystal surface with formation of defect-like vacancies and complexes (voids) which cause the formation of surface hillocks.

(v) Surface sintering and merging of particles inside small clusters.

The reorganized pattern comprises the left- and the right-tilted rhombic clusters, stretched-clusters with isosceles triangular lattice, and the zig-zag type clusters (Fig. 3a). Such clusters are formed by the strong local shear when the particles of regular clusters are put in motion, as schematically shown in the inset of Fig 3b. The reorganization is initiated once the Coulomb repulsion between the particles overcomes the friction force thus putting them in motion similar to the case described above. However, there is some difference because another process also takes place. Namely, the surface softening of the silicon substrate and of the silica particles occurs

due to the fact that ion bombardment causes ion-induced viscous flow, as shown by a number of authors for a wide range of ion energies [25-27]. Mayer *et al.* [26] have found that bombardment of SiO_2 with light H and He ions at energies between 0.2 – 1 eV causes viscous flow leading to surface smoothing. This process is first order type with ion fluence and strongly dependent on the ion energy in the mentioned energy range. They measured the ion–induced viscosity of SiO2 and found its values in the order of 1 – 20 x 10^{12} Nsm^{-2} [26]. The viscous-flow term is responsible for surface smoothing and softening and it can be found by solving the 2D Navier-Stokes equation, assuming one of the two limiting cases: (i) viscous flow which extends from the surface layer into the bulk (unconfined flow) [25,27]; (ii) viscous flow which is confined only to the surface layer [25].

Umbach *et al.* [25] have found that bombardment of SiO_2 with Ar ions in the energy range 0.5 - 2 keV causes significant viscous flow that occurs in the surface layer with a depth on the order of the ion penetration range (< 5 nm). Here macroscopic stress relaxation, called ion-induced viscous flow - (measured on thick and thin films) in the low and medium temperature range (from the room temperature up to 200 ^{0}C), occurs through surface

rearrangements dominated by the atomic collision-cascade process [25]. This temperature dependent viscous flow below 200^{o}C shows linear dependence; while above this temperature it shows a nonlinear Arrhenius-type behavior [25]. It was also shown that ion-enhanced diffusion is negligible with respect to ion-induced viscous flow.

The conclusion about ion-induced viscous flow based on the above described experimental and theoretical results can be applied to our case both for the silica particles and the silicon substrate exposed to the ion energy of 40 keV. Thus, we may assume that the silicon viscous flow layer is formed in which the silica particles are embedded.

In that case the Coulomb force which should move the soft particles on the soft substrate becomes insufficent to cause the reorganization. Instead, the softening of the silicon surface and shear flow, as well as the interaction of particles with the fluid silicon layer play the crucial role in LB layer reorgnization. The motion of particles in a viscous silicon layer causes the compactification of clusters by lateral compression in some domains, and rarefaction in other domains (Fig.3c). In the domains of rarefaction, the formation of wide defect-channels takes place so that a large surface area of silicon is exposed to the ion beam. In the compactified domains of this

fluid/solid system, however, local jamming takes place, similarly to that is observed in colloidal suspensions [28], granular systems [29-31] and traffic [32], thus indicating variation of shear rates and shear viscosity over the LB layer.

At the fluence of $\Phi = 10^{17}cm^{-2}$, the large clusters break into small ones of 4, 3, or 2 particles and mostly into a set of single isolated particles (Fig.4). The process is associated with largely intermittent particle distribution and formation of wide defect-channels of ~200 – 300 nm between the clusters. However, the onset of 2D surface flow of the silicon viscous layer is more intense in the wide defect-channels and is less intense in the narrow defect-channels. The reorganization leads to the formation of intermittent strings of particles which form closed (finite) and open (infinite) loops. Such chain-loops are clearly seen if the particles shown in Fig. 4 are connected by the red lines. The reconstruction of the chain-like particle organization at the highest fluence indicates the effects of quasi 2D-turbulent flow field with elongated streamlines.

Figure 5 shows few configurations of the silica particles with solidified surface which was in the viscous state during the ion irradiation process. Fig. 5a shows different stages of two particle connection; fomation of a neck

between the particles (Fig. 5a(i)), formation of bridges as wide stripes between the particles (Fig. 5a(ii)), and the full merging of particles (Fig. 5a(iii)). Figure 5b shows various stages of the connection of three particles; the SEM micrograph of 3 particles connected by necks (Fig. 5b(i)), bridges (Fig. 5b(ii)), and finally the complete merging of the particles (Fig. 5b(iii)). Conspicuously, the AFM analysis at large magnification reveals that merged particles comprise two types of small holes. The first type (Fig. 6(i)) are sharp holes of ~20 nm in diameter which make a rough (sponge-like) silica surface (Fig. 6(ii)). The reason may be the formation of bubbles in the material due to the high atomic concentration of implanted noble gas atoms. These subsurface bubbles can cause even a full exfoliation of the top surface layer of the particle. In other cases (when the bubble concentration does not exceed its critical value), only few cavities are formed by the gas bubble ejection through the particle surface.

Another type of holes are circular craters of 30 – 50 nm in diameter with a toroidal ring on their rim, see Fig. 6(iii). They may be formed by abrupt release of Ar from molten silica particles as found in our previous work where the detected amount of argon in the spheres was found to be several times lower than it was expected from the irradiation fluences [33].

However, at the same time no such discrepancy of the Ar content, i.e., no escape of Ar was found for the Si substrate.

3.2.2 *Large size particles*

The ion irradiation of the LB layer of large size particles (D = 450 nm), does not cause significant reorganization as compared to the case of medium size ones (Fig. 1b). Ion irradiation at $\Phi = 1 \times 10^{15} cm^{-2}$ transforms the 2D large rhombic grains of densely packed particles into smaller grain clusters of about 2 μm × 2 μm size with narrow defect-channels of about 80 – 100 nm width as it is shown in the AFM micrographs in Figs. 7a(i,ii).

Increasing the fluence to $\Phi = 5 \times 10^{15} cm^{-2}$ causes the reorganization of the large (rhombic) grains into smaller ones of about 1.5 μm × 1.5 μm in size with the formation of 150 – 200 nm wide defect-channels, connected under 60^{o} (Fig. 7b(i)). Buckling of the particles causes the formation of necks between them. Fig. 7b(ii) shows the AFM micrograph of the Si surface after ion irradiation through the mask of silica particles.

At higher fluences between $10^{16} cm^{-2}$ and $5 \times 10^{16} cm^{-2}$ the particle diameter decreases down to D ~ 430 nm that indicates the possible onset of sputtering (Fig. 8a(i)). The decrease of the particle diameter is accompanied by the

increase of the width of the defect-channels thus exposing larger silicon area to the ion beam. Figure 8a(ii) reveals the channel-defects which become wide and ramified.

Above the fluence of $5\times10^{16}cm^{-2}$, further decrease of the particle diameter to ~ 420 nm, and increase of the size of defect-channels with the change of morphology can be observed (Figs. 8b(i,ii)). The variation of the Si swelling morphology follows increase of the ion fluence. At high fluence, a strong swelling forms walls around the particles so that they are restricted to move.

The analysis of the AFM micrographs in Figs. 7 and 8 reveals that the increase of the swelling amplitude vs. the ion fluence can be represented by two diagrams; one for wide defect-channels (between the clusters), and another for narrow defect-channels (inside the clusters), as shown in Fig. 9. In the first case the swelling is nonlinear and can be approximated by two linear regions in the fluence ranges (i) $10^{15}cm^{-2}$ – $5\times10^{16}cm^{-2}$ and (ii) $5\times10^{16}cm^{-2}$ – $10^{17}cm^{-2}$, respectively. The highest swelling amplitude of ~70 nm in the range (ii) is much larger than reported by Giri *et al.* [34]. The mechanisms of swelling in the narrow channels with dense regular packing of particles cannot give such strong amplitude growth as in the case of wide defect-channels with inhomogeneous particle packing. The linearly growing

amplitude in Fig. 9 for small inter-particle distances reaches ~ 40 nm at the maximum, being comparable to the results of Lindner *et al.* [11] and Nagy *et al.* [7].

The phenomenon of linear silicon swelling has been semi-empirically modeled in Ref. [7] upon considering proximity effects. The most significant Si swelling occurs when the local fluence between the particles is equal or close to the irradiation input. At the particle edges, however, there is a fluence transition region which can be narrower or wider, depending on the ion energy, particle diameter and the average inter-particle distance. The swelling profile significantly depends on the ratio between the transition region and the inter-particle distance [7].

The AFM micrographs in Figs. 7 and 8 reveal swelling spikes and interconnected rims. The spikes emerge between free adjacent particles which are interconnected by necks thus forming a triangular “bridge” [7, 11]. This triangular "bridge" also acts as mask and prevents the underlying Si surface from significant swelling. On the other hand, the swelling rims appear in the regions of no neck formation.

3.3 Characteristics of particle charging, discharging, and ion irradiation-induced viscous flow

The reorganization of the monolayer of silica nanoparticles is the result of Coulomb interaction due to particle charging, and of the particle and substrate softening due to ion irradiation-induced viscosity. The instantly excited volume of particles (depending on the ion penetration range) determines the charging effects through the excitation of the target atoms by ions and recoils, secondary electron emission, as well as ion beam-induced sputtering. The penetration range in the silica particles was estimated by full-cascade Stopping and Range of Ions in Matter (SRIM) simulations performed for 40 keV Ar^+ ions.

3.3.1 Charging effects

As it has been detailed in Ref. [6] and [35], the charging of particles can be estimated on the basis of the equation:

$$\frac{dQ_h}{dt} = (1+\gamma_e)\Phi eP \qquad (1)$$

where Q_h is the surface hole density, γ_e is the secondary ion-electron emission coefficient in silica, Φ is the ion fluence, e is the elementary

charge, and P is the probability for hole endurance in the silica particle. The surface charging as a function of time is given by [6, 35]

$$Q_h = \frac{4(1+\gamma_e)eP_0R_p}{7\left(1+\frac{\Phi(t)}{\Phi_0}\right)\mathrm{Y}\Omega_0}\left(1-e^{-7\Omega_0\Phi(t)/4R_p}\right). \qquad (2)$$

Here Φ_0 is the characteristic fluence for which the concentration of newly created dangling bonds (shallow traps) is equal to their concentration prior to the irradiation, Ω_0 is the average volume of an atom, R_p is the ion penetration range, Y is the sputtering yield, and P_0 is the probability for hole preservation in the unirradiated film [6, 35, 36]. Here Φ_0, R_p, Y, and γ_e were considered as $\Phi_0 \sim 2\times10^{12}/\mathrm{cm}^2$ [6], R_p = 47 nm, Y = 2.7, and γ_e, = 0.25, respectively. Assuming P = 1, i.e., no leakage of holes Q_h *vs* Φ is obtained as the analytical solution of Eq. (2). The results can be seen in Fig. 10a.

Considering the maximum charges in Fig. 10a, the local electric field built around the particles is estimated to be 1-10 MV/cm. For such a high field, the leakage of holes from the particles to the Si substrate may be significant. See, e.g., another detailed study on plasma-chemical synthesis and electric-charge-driven self-organization of SiO_2 nanodots [36]. Considering the electric field-induced leakage and tentatively assuming the

leak of holes to be 30 % (P = 0.7), one can find the total charge densities Q = $Q_h D^2\pi/4$, which are presented in Fig. 10a by the light blue and pink curves.

The Coulomb repulsive force, F_C, is simply estimated from the particle charge and the interaction between two adjacent particles [6]. The force F_C (without leak of holes) as the function of fluence for medium and large-size particles is given in Fig. 10b (by the red and dark blue curves, respectively). Taking into account the leak of holes as 30% gives the correction to the Coulomb force as it is shown in Fig. 10b.

The analysis of particle motion requires comparison of the repulsive Coulomb force F_C and the friction force F_{frict} which were estimated in Ref. [6]. At low fluences, below 5×10^{16}cm^{-2}, when charging is high, the system behaves as the "solid particles on the solid substrate". Figure 10b shows that the Coulomb repulsive force F_C is an order of magnitude larger than the friction force for both D = 220 nm and D = 450 nm particles. Therefore F_C may cause particle motion and reorganization, similarly to that was found for Ga^+ ion irradiation [6].

3.3.2. Thermal effects

Besides charging effects, also thermal effect should be considered, like surface 2D melting that occurs at the characteristic 2D melting temperature Θ [6]. Assuming that $\Theta \sim (0.6–0.7)T_M$, (T_M = bulk melting point) [37], one finds for the silica particles (with T_M = 2000 K), that Θ(Silica) ≈ 1200 K, while for the silicon substrate (with T_M = 1683 K), that Θ(Silicon) ≈ 1000 K, respectively. As mentioned in the Experimental section, the Ar^+ beam power density is several orders of magnitude lower than that was for Ga^+ ion irradiation, so that heating by the Ar^+ beam cannot reach the temperature of 2D melting. Namely, assuming an input power of P_{in} = 1 W/cm^2, and steady state between P_{in} and heat radiation from the particles, the maximum temperature increase is estimated to be less than 100^{o}C.

3.3.3. Irradiation-induced flow and fluid dynamics

The high fluence of $\Phi = 5\times10^{16}$cm^{-2} causes swelling and ion beam-induced viscous flow of the Si surface [25-27]. A significant surface swelling largely increases the contact area between the particles and the Si substrate thus increasing the particle-substrate adhesion forces. The system behaves as the “solid particles on the fluid-like substrate”, so that the motion

of particles is governed by the fluid-like Si layer in which reorganization occurs by the Brownian motion similar to the colloidal suspension of solid particles.

An even higher fluence of $\Phi = 1\times10^{17}$cm^{-2} causes ion-induced viscous flow on both, the particle surface and on the Si substrate surface, so that the system behaves as the "soft particles on the fluid-like substrate" [6]. In this case, the reorganization occurs by the action of both, hydrodynamic interactions between the particles and interactions of particles with the liquid-like silicon surface.

The above conclusion about motion of particles in the fluid-like silicon layer makes possible to establish connection with the system of colloidal suspension of fluid-like particles. In this respect, the dynamics of silica particles can be interpreted on the basis of dynamics of two types of colloidal suspensions (i) the suspension with Brownian motion of solid spheres which ignores fluid dynamic interactions between the particles, in the first case; (ii) the suspension with interaction between the fluid-like particles, in the second case. For both types of colloidal suspensions, the description by 2D Navier-Stokes (NS) equation in the frame of the Tanaka-Araki model [38] is the most appropriate one.

This hybrid Tanaka-Araki model combines a lattice simulation for continuous field (solvent) and an off-lattice simulation for particles. The suspension is assumed as viscous fluid particles with viscosity η_c which are suspended in a liquid with viscosity η_s. Defining the parameter $R = \eta_c/\eta_s$, one can describe the *system of fluid particle suspension for* $R \rightarrow 1$, and the *system of solid particle suspension for* $R \rightarrow \infty$. In the most general case, a fluid particle with the center of mass located at $\boldsymbol{r}_i$ is represented by the concentration fields [38]:

$$\phi_i(\boldsymbol{r}) = [\tanh\{(a - |\boldsymbol{r} - \boldsymbol{r}_i|)/\xi\} + 1]/2 \quad , \tag{3}$$

where a is the particle radius and ξ is the interface thickness. The spatial distribution of the viscosity is given by $\eta(\boldsymbol{r}) = \eta_s + \Sigma_i^N \Delta\eta\phi_i(\boldsymbol{r})$, where $\Delta\eta$ is the viscosity difference between the liquid and suspension, and $\eta_c = \eta_s + \Delta\eta$. The inter-particle potential $V(r)$ is assumed to be [38]:

$$V(r) = k[(\sigma/r)^{12} - (\sigma/r)^6], \tag{4}$$

where k is the strength of the potential and σ is the range of interaction [38]. The force acting on the i-th particle is $\mathbf{F}_i = -\partial / \partial \boldsymbol{r}_i \left[\Sigma_{i\neq 1}^{N} V(|\boldsymbol{r} - \boldsymbol{r}_i|)\right.$, while the continuous force fields are $\mathbf{F}(r) = \Sigma_i^N \mathbf{F}_i \phi_t(\boldsymbol{r})$. The dynamics of suspended system is described by the Navier-Stokes equation (NS) [38]:

$$\rho(D/Dt)\boldsymbol{v} = \mathbf{F} - \nabla p + \nabla \cdot [\eta\{\nabla \boldsymbol{v} + (\nabla \boldsymbol{v})^t\}] + \xi \quad , \qquad (5)$$

where $D/Dt = \partial / \partial_t + \boldsymbol{v} \cdot \nabla$, ρ is the density, and ξ is the thermal force noise. The nonlinear term $\rho \boldsymbol{v} \cdot \nabla \boldsymbol{v}$ and the noise term ξ are neglected for simplicity. The simulation is performed by the solution of Eq. (5), and the velocity fields at any moment t +Δt are incremented by [38]:

$$\rho \nabla \boldsymbol{v} = [\, \mathbf{F} - \nabla p + \nabla \cdot \{\eta(\nabla \boldsymbol{v} + (\nabla \boldsymbol{v})^t\}]\Delta t \quad , \qquad (6)$$

using the time domain Δt. The solution of the equation gives the new distribution of particles after Δt, with the new fields of ϕ and $\boldsymbol{v}$ on the lattice. With these fields, one has to solve Eq. (5) again. Repetition of this procedure

for every new Δt, gives the space-time development of the particle reorganization as well as of the continuous velocity field [38].

The simulation of particle dynamics is based on the assumption that the single particle is moving with constant velocity $\boldsymbol{v}_0$ relative to the surrounding fluid, and the colloidal system is characterized with the viscosity ratio R [38].

(i) The dynamics of the "solid silica particles on the soft silicon substrate", can be described by the dynamics of the corresponding solid particles colloidal suspension assuming a drain-free case (no hydrodynamic interaction between the particles). Here Eq. (5) is reduced to [38]:

$$\rho \partial / \partial_t \boldsymbol{v}_i = \mathbf{F}_i - f \boldsymbol{v}_i \quad , \tag{7}$$

where f is the friction constant ($f = (1/3)10^4$ in nondimensional units). The simulation of Brownian dynamics by the above described Tanka-Araki procedure for $R = 50$ (equivalent to $R \rightarrow \infty$), gives the particle reorganization in time $t + \Delta t$ with $\Delta t = 0.01$, as shown in Fig. 11a. The resulting rhombic, stretched rhombic, trapezoidal, and joined rhombic clusters which evolve

after (nondimensional) time t = 200 – 1000 are similar to the clusters of medium size silica particles shown in Figs. 3 and 4.

(ii) The dynamics of the "soft silica particles on the soft silicon substrate" can be described by Eq. (5) for the fluid-like colloidal particle suspension with R = 1, assuming hydrodynamic forces between the particles. The resulting simulation gives the long chain-like particle organization. Starting from the same homogeneous particle distribution as for (i), the reorganization leads to the formation of compact chains in which the particles stick together along the whole chain length (Fig. 11b). These chain-particle formations can be compared to the chains of silica particles shown in Fig. 4.

In summary, the reorganized pattern of polygonal clusters of medium size particles in Fig. 3 is similar to the pattern in Fig. 11(a); while the reorganized large chains of particles in Fig. 4 are similar to those in Fig. 11(b). This tendency is also reflected in the different cluster sizes formed at the higher irradiation fluences, as it is shown in the next section.

3.3.4. Particle cluster size

The analysis of the reorganized patterns reveals the decrease of the cluster size N (number of particles in the cluster) with increasing the ion fluence, see Fig. 12. The medium size particles of diameter D = 220 nm tend to form small clusters with decreasing size from N = 12 to N = 2, ultimately tending to a single (isolated) particle. The clusters of large size particles behave similarly, however, the cluster size decreases from N = 26 to $N \leq 10$ at $\Phi \geq 5\times10^{16}\text{cm}^{-2}$. For the highest fluence, N seems to stay constant or decreases very slightly.

The tendency of large particles to form clusters of bigger size within the whole fluence range is the consequence of their lower mobility at lower fluences (due to the weak Coulomb repulsion), and of the lower mobility on the liquid-like silicon surface at higher fluences (due to the higher friction force).

4. CONCLUSIONS

The Ar^+ ion beam-induced reorganization of a Langmuir-Blodgett monolayer of medium and large size silica particles has been investigated in

a wide ion fluence range. The reorganization process, cluster formation, charging, discharging, ion-induced viscous flow as well as substrate swelling has been found to depend on a number of parameters: ion fluence, particle size, inter-particle distance, the density of particle packing, and the initial self-organization of particles in the LB layer. The widening of the defect-channels between the particle clusters causes the compression and jamming of particles inside the clusters.

The observed reorganization features of an inhomogeneous monolayer of medium and large size silica particles are characteristic for the applied ion fluence range. At low fluences, the system behaves as the "solid particles on the solid substrate" and the reorganization is mainly driven by charging and Coulomb repulsion forces. At higher fluences hole leakage and discharging may occur and, due to the ion beam-induced viscous surface flow of silicon, the behaviour of particles can be considered as the colloidal suspension of "solid particles on the soft substrate". The reorganization occurs by Brownian motion and causes the formation of rhombic, trapezoidal and zig-zag clusters. On the other hand, considering the ion beam-induced viscous-flow also for the particles, the system behaves as the "soft particles on the soft substrate" being equivalent to fluid particles in a fluid layer. In that case, the reorganization is driven via long-range hydrodynamic particle-particle

interactions and causes the formation of chain-clusters of densely packed particles. The dynamics of the particle reorganization process in both cases is treated analogous to the dynamics of a colloidal suspensions based on the Tanaka-Araki model. The results of the reorganization process in such colloidal suspensions are comparable to the experimentally observed cluster distributions in both cases.

Acknowledgements

The authors are thankful to Mrs. Eszter Gergely-Fülöp for preparation of the Langmuir-Blodgett layers and to Ábel Debreczeny for performing ion implantation. Support from the project 098-0982904-2898 of the Croatian Ministry of Science, Education and Sport, and from the Hungarian Research grants OTKA PD 105173, and OTKA K 112114 is highly appreciated. A. D. is supported by the János Bolyai Research grant of the Hungarian Academy of Sciences.

REFERENCES

[1] U. Diebold, The surface science of titanium dioxide, Surf. Sci. Rep. **48** (2003) 53 - 229.

[2] G. Subramanian, V. N. Manoharan, J. D. Thorne, D.J. Pine, Ordered Macroporous Materials by Colloidal Assembly: A Possible Route to Photonic Bandgap Materials, Adv. Mater, **11** (1999) 1261- 1265.

[3] T. van Dillen, A. Polman, W. Fukarek, A. van Blaaderen, Energy-dependent anisotropic deformation of colloidal silica particles under MeV Au irradiation, Appl. Phys. Lett, **78** (2001) 910 - 912.

[4] M. Skupinski, R. Sanz, J. Jensen, Surface patterning by heavy ion lithography using self-assembled colloidal masks, Nucl. Instr. Meth. Phys. Res. **B 257** (2007) 777- 781.

[5] S. Lugomer, Z. Zolnai, A. L. Toth, I. Barsony, Self-organization of silica nano-particles induced by the ion beam, Physica Status Solidi, **C 8** (2011) 2858–2861.

[6] S. Lugomer, Z. Zolnai, A. L. Toth, I. Barsony , A. Maksimović and N. Nagy, Reorganization of Langmuir-Blodgett layers of silica nanoparticles induced by the low energy, higfh fluence ion irradiation, Thin Solid Films, **520** (2011) 4046 - 4056.

[7] N. Nagy, Z. Zolnai, E. Fulop, A. Deak and I Barsony, Tunable ion swelling for nanopatterning of macroscopic Surfaces: The role of proximity effects, Appl. Surf. Sci, **259** (2012) 331- 337.

[8] H. J. Withlow, M. Ling Ng, V. Auzelyte, I. Maximov, I. Montelius, J.A.Van Kan, A.A. Bettiol, W. Fatt, Lithography of high spatial density biosensor structures with sub-100 nm spacing by MeV proton beam writing with minimal proximity effect, Nanotechnology, **15** (2004) 223 - 226.

[9] H. Xu, S. Melle, K. Golemanov G. Fuller, Shape and Buckling Transitions in Solid-Stabilized Drops, Langmuir, **21** (2005) 10016 - 10020.

[10] C. Quilleiet, Depressions at the surface of an elastic spherical shell submitted to external pressure, Phys. Rev E **74** (2006) 046608(1)-046608(6).

[11] J.K. N. Lindner, C. Seider, F. Ficher, M. Weinl and B. Stritzker, Nanosphere lithography for device fabrication, Nucl. Instr. Meth. Phys. Res B, **267** (2009) 1394 – 1397.

[12] E. Chason, J. Y. Tsao, K. M. Horn, S.T.Picraux, H. A. Atwater, Surface roughening of Ge (001) during 200 eV Xe ion bombardment and Ge molecular beam epitaxy, J. Vac. Sci. Tech. A **8** (1999) 2507 – 2511.

[13] M.Werner, J. Van den Berg, Jakob, D. G. Armour, G. Carter, T. Feudel, M. Herden, M.Bersani, D. Giubertoni, L. Ottaviano, C. Bongiorno, G. Mannino, P. Bailey, T.C.Q. Noakes, Shallow BF[sub 2] implants in Xe-bombardment-preamorphized Si: The interaction between Xe and F, Appl. Phys. Lett., **86** (2005) 151904 - 151906.

[14] Z. Zolnai, A. Deak, N. Nagy, A. L. Toth, E. Kotai, G. Battistig, A 3D-RBS study of orradiation-induced deformation and masking properties of ordered colloidal n anoparticulate masks, Nucl. Instr. Meth. Phys. Res, **B 262** (2010) 79 - 86.

[15] T.van Dillen, E. van der Giessen , P.R. Onck and A. Polman, Size-dependent ion-beam-induced anisotropic plastic deformation at the nanoscale by nonhydrostatic capillary stresses, Phys. Rev. **B 74** (2006) 132103(1)- 132103(4).

[16] J. K. N. Lindner, B. Gehl, B. Strityker, Nanosphere lithography for device fabrication, Nucl. Instr. Meth. Phys. Res, **B 242** (2006) 167 - 169.

[17] T. van Dillen, A. van Blaadern, A. Polman, Shaping of colloidal assemblies, Materials Today, July/August (2004) 40 - 46.

[18] W. Stöber, A. Fink, and E. Bohn, Controlled growth of monodisperse silica spheres in the micron size range, *J. Colloid Interface Sci.* **26** (1968) 62 - 69.

[19] M. Szekeres, O. Kamalin, R. A. Schoonheydt, K. Wostyn, K. Clays, A.Persoons and I. Dekany, Ordering and optical properties of monolayers and multilayers of silica spheres deposited by the Langmuir–Blodgett method, J. Mater. Chem, **12** (2002) 3268 - 3274.

[20] H. Okudera, A. Hozumi, The formation and growth mechanisms of silica thin film and spherical particles through the Stöber process, Thin Solid Films, **434** (2003) 62 -68.

[21] C.A.P. Leite, E.F. de Souza, F. Galembeck, «Core-and-shell nature of Stober Silica Particles», J. Braz. Chem. Soc.,12 519-525 (2001).

[22] H. Ryssel, L. Frey, V. Haublein, M. Lucassenand J. Gyulai, «An analythical model for beam induced contamination in uion implantation», Proceedings of the Int. Conf. on Ion Implantation Technology, Kyoto, 1998, p. 498-501.

[23] N. J. Wagner and J. F. Brady, Shear thickening in colloidal dispersions, Phys. Today, Oct. (2009) 27 - 32.

[24] C. O. Osuji, C. Kim , D. A. Weiz, Shear thickening and scaling of the elastic modulus in a fractal colloidal system with attractive interactions, Phys. Rev. E **77** (2008) 060402(1) - 060402(4).

[25**]** C. C. Umbach, R. L. Headrick, K-C. Chang, Spontaneous nanoscale corrugation of ion-eroded SiO2: The role of ion-irradiation-enhanced viscous flow, Phys. Rev. Lett., **87** (2001) 246104(1) - 246104(4)

[26] T. M. Mayer, E. Charson, A. J. Howard, Roughening instability and ion-induced viscous relaxation of SiO2 surfaces, J. Appl. Phys., **76** (1994) 1633-1643.

[27] G. Carter, Effect of surface-height derivative processes on ion-bombardment-induced ripple formation, Phys. Rev. B **59** (1999) 1669-1672.

[28] J. M. V. A. Koelman, P.j. Hoogerbugge, Dynamic simulations of hard-sphere suspensions under steady shear, Europhys. Lett., **21** (1993) 363 - .

[29] S. H. E. Rahbari, J. Vollmer, S. Herminghaus, M. Brinkman, A response function perspective on yielding of wet granular matter, EPL Frontiers in Physics, **87** (2009) 14002(1) - 14002(6).

[30] H. A. Makase, D. L. Johnson, L. M. Schearz, Packing of compressible granular materials, Phys. Rev. Lett, **84** (2000) 4160 - 4163.

[31] T.S. Majumdar, R.P. Behringer, Contact force measurements and stress-induced anisotropy in granular materials, Nature, **435** (2005) 1079 - 1082.

[32] T. Nagatani, The physics of traffic jams, Rep. Prog. Phys., **65** (2002) 1331- 1386.

[33] Z. Zolnai, N. Nagy, A. Deák, G. Battistig, E. Kótai, Three-dimensional view of the shape, size, and atomic composition of ordered nanostructures by Rutherford backscattering spectrometry , Phys. Rev. **B 83** (2011) 233302(1) -233302(4).

[34] P. K. Giri, V. Raineri, G. Franzo, E. Rinimi, Mechanism of swelling in low-energy ion-irradiated silicon, Phys. Rev. **B 65** (2001) 012110(1) - 012110(4) .

[35] S. Yogev, J. Levin, M. Molotskii, A. Schwarzman, O. Avayu and Y. Rosenwas, Charging of dielectrics under focused ion beam irradiation J. Appl. Phys. **103** (2008) 064107(1) – 064107(6).

[36] Based on the arguments of Yogev *et al* [38], under low fluence irradiation, when $\Phi < \Phi_0$, the surface charge density Q_h is proportional to Φ due to the increase in the number of the excited holes (the concentration of which rapidly increases with the ion fluence) [38]. At higher fluence, the surface charge density Q_h, decreases as ~$1/\Phi$ due to the generation of a large number of shallow hole traps that decreases the probability for hole capture in deep traps.

[37] R. Zito, Surface and grain boundary diffusion, Thin Solid Films, **60** (1979) 27 -31.

[38] H. Tanaka,T. Araki, Simulation method of colloidal suspensions with hydrodynamic interactions: Fluid particle dynamics, Phys. Rev. Lett., **85** (2000) 1338- 1341.

FIGURE CAPTIONS

Fig.1. (Color online) SEM micrographs of self-organized LB layers of silica nanoparticles.

a) Particle diameter D = 220 nm; Insets- top right: small zig-zag connected rhombic clusters; bottom left: chevron-type cluster of three connected hexagons.

b) Particle diameter D = 450 nm; Insets- top right: rhombic cluster, bottom right: irregular particle organization.

Fig.2. (Color online). Reorganized LB layer of silica nanoparticles with diameter D = 220 nm at various fluences: (a) $\Phi = 10^{15} - 5\times10^{15}\text{cm}^{-2}$; (b) $\Phi = 10^{16}\text{cm}^{-2}$.

Fig.3. (Color online). Reorganized LB layer of silica particles with diameter D = 220 nm irradiated to a fluence of $\Phi = 5\times10^{16}\text{cm}^{-2}$.

a) SEM micrograph showing left-tilted and right-tilted rhombic and the zig-zag clusters.

b) Schematics of the reorganization process of particle clusters due to the quasi-2D turbulent flow of softened silicon.

c) Jamming of silica particles in disordered clusters.

Fig.4. (Color online). Reorganized LB layer of silica nanoparticles with diameter of D = 220 nm irradiated to a fluence of $\Phi = 10^{17}cm^{-2}$. SEM micrograph reveals small clusters of 2 or 3 particles, larger clusters of 5 to 6 particles, and the chain-clusters of particles.

Fig.5. (Color online). Merging of silica particles into clusters after irradiation to a fluence of $\Phi = 10^{17}cm^{-2}$.

a. SEM micrograph of a two-particle-cluster: Particles connected by neck (i); and by bridge (ii); and merged particles (iii).

b. SEM micrograph of a three-particle-cluster: particles connected by neck (i); by bridge (ii); and merged particles (iii).

Fig.6. SEM micrograph of three merged particles after irradiation to a fluence of $\Phi = 10^{17}cm^{-2}$. Merged particles reveal two types of holes on the surface (i and iii). Small irregular holes with sharp edges (ii); Large circular holes with toroidal rim (iv).

Fig.7. (Color online). The effects of Ar^+ ion irradiation on the reorganization of the LB layer of silica particles of D = 450 nm, and on the underlying silicon substrate at various ion fluences.

(i) SEM micrograph of silica particles; (ii) AFM micrograph of the Si surface irradiated to a fluence of (a) $\Phi = 10^{15}cm^{-2}$; (b) $\Phi = 5\times10^{15}cm^{-2}$.

Fig.8. (Color online). The effect of Ar^+ ion irradiation on the reorganization of the LB layer of silica particles of D = 450 nm, and on the underlying silicon substrate at various ion fluences.

(i) SEM micrograph of silica particles; (ii) AFM micrograph of the Si surface irradiated to a fluence of (a) $\Phi = 5\times10^{16}cm^{-2}$; (b) $\Phi = 10^{17}cm^{-2}$.

Fig.9. (Color online). Swelling amplitude *vs* ion fluence: (i) Nonlinear silicon swelling inside wide defect-channels between the clusters; (ii) Linear silicon swelling inside narrow channels between closely packed particles.

Fig.10. (Color online). Estimation of the number of holes/particle (particle charge), the Coulomb force between two adjacent particles, Fc, and the

friction force, F_{frict}, as function of the ion fluence for D = 220 nm and 450 nm particles.

(a) Charging of silica particles as function of the ion fluence: Assuming no leakage of holes to the substrate (dark blue curve: D = 220 nm; red curve D = 450 nm) ; Assuming 30 % leakage of holes to the substrate (light blue curve D = 220 nm ; pink curve: D = 450 nm).

(b) The Coulomb force for both types of particles is larger than the friction force and may cause their motion on the Si surface. (upper segment of Fig 11. b shows the relation between the forces at larger magnification).

Fig.11. (Color online). Results of numerical simulation of the reorganization process for a colloidal suspension of particles starting from an initially homogeneous phase.

a) Brownian-dynamics-like simulation based on Eq. (7), considering no hydrodynamic interaction between the particles.

b) "Fluid particle dynamics" simulation based on Eq. (5), considering hydrodynamic interaction between the particles. (Courtesy of H. Tanaka, from: H. Tanaka and T. Araki, Phys. Rev. Lett, **85** (2000) 1338; By permission of APS, Copyright APS 2000).

(http://dx.doi.org/10.1103/Phys.Rev.Lett85.1338)

Fig.12. (Color online). Particle cluster size as function of the Ar ion fluence for D = 220 nm and D = 450 nm particles.

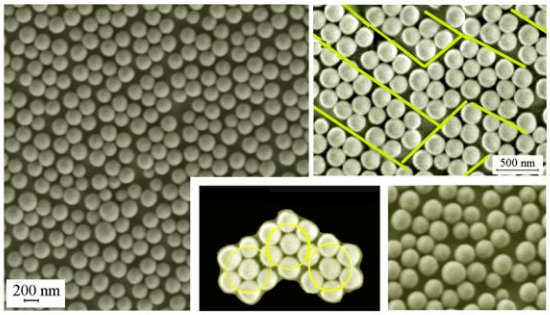

(a)

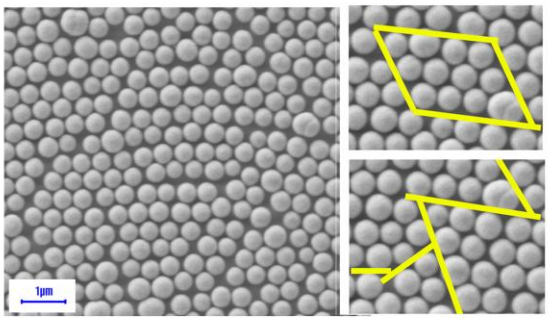

(b)

Fig. 1.

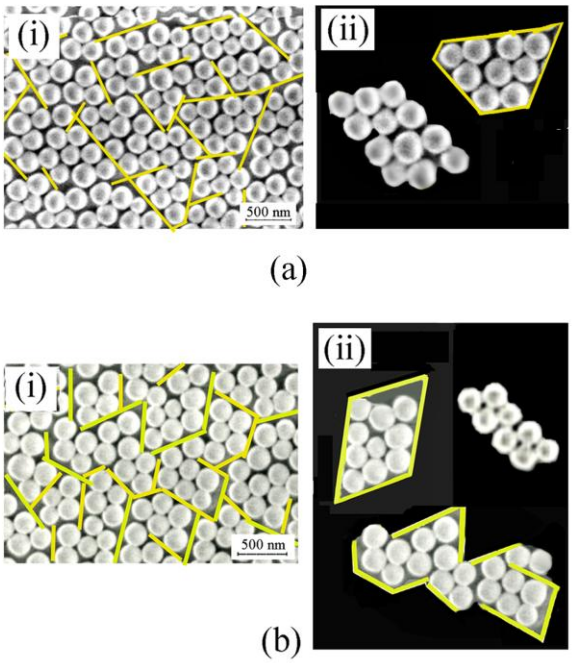

Fig.2.

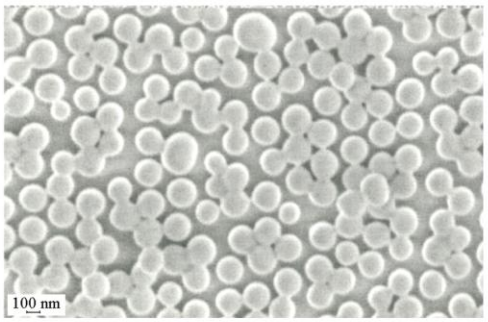

(a)

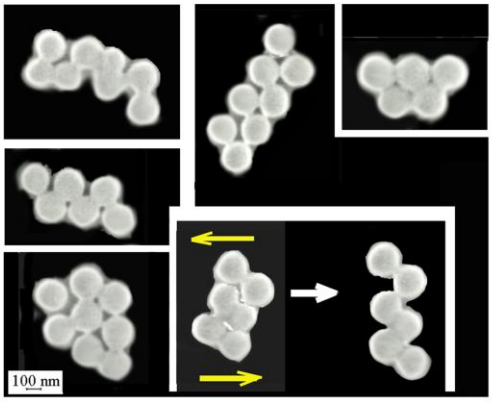

(b)

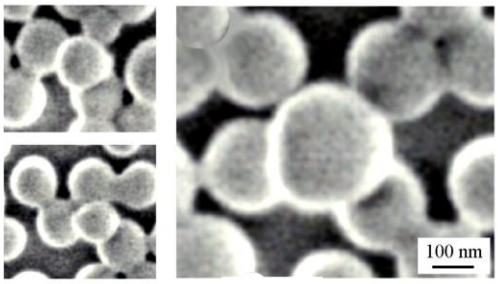

(c) 100 nm

Fig.3.

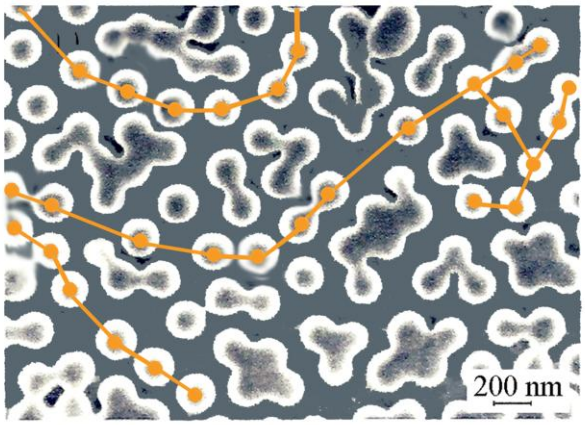

Fig. 4.

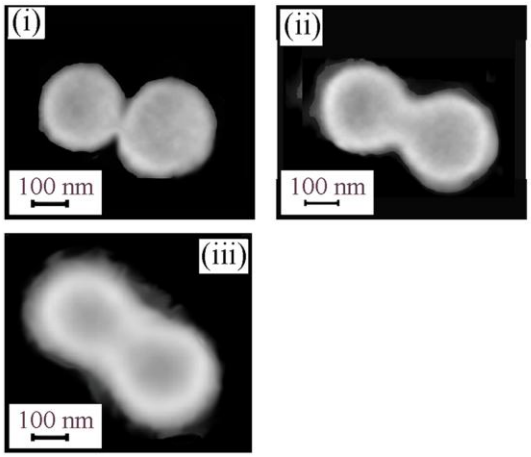

(a)

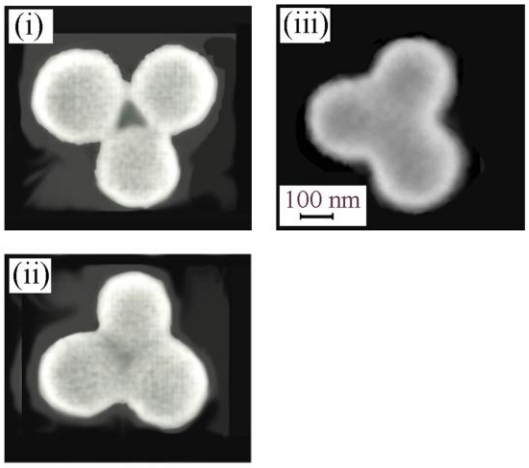

(b)

Fig. 5.

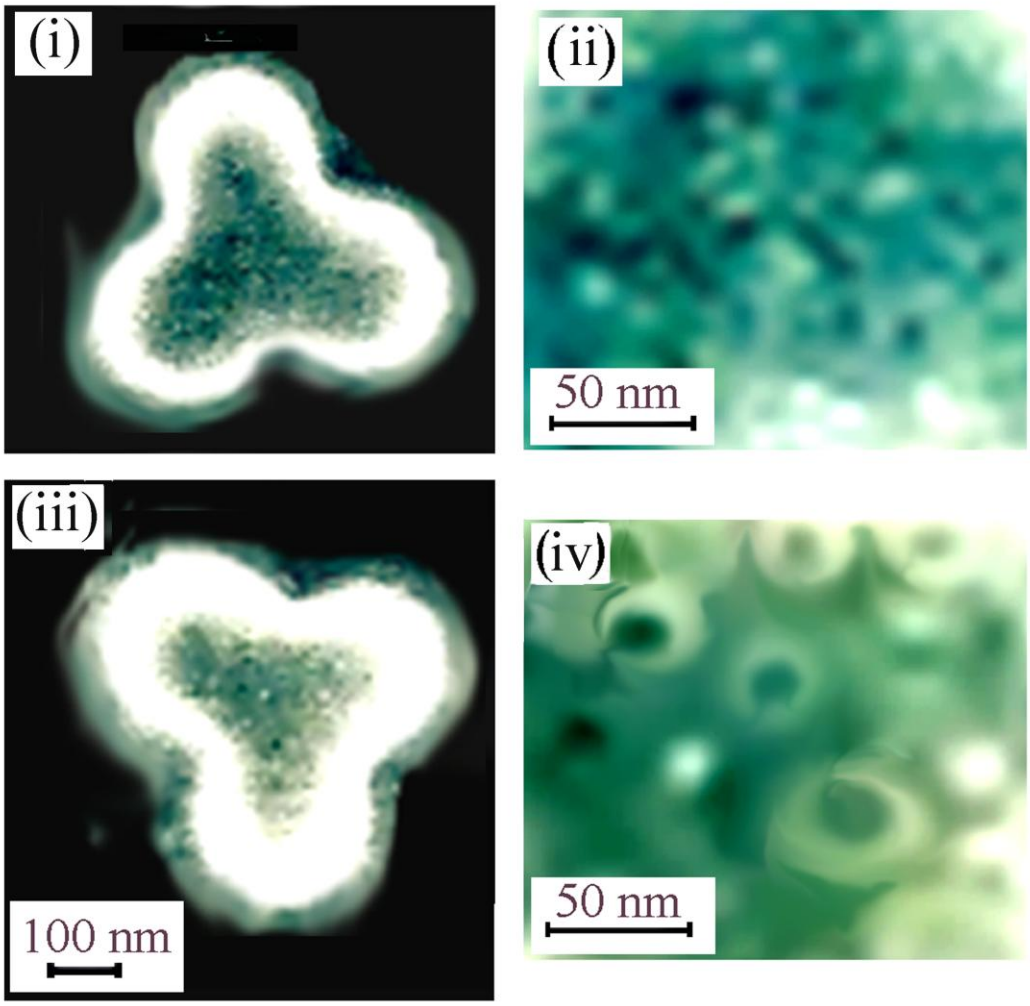

Fig. 6.

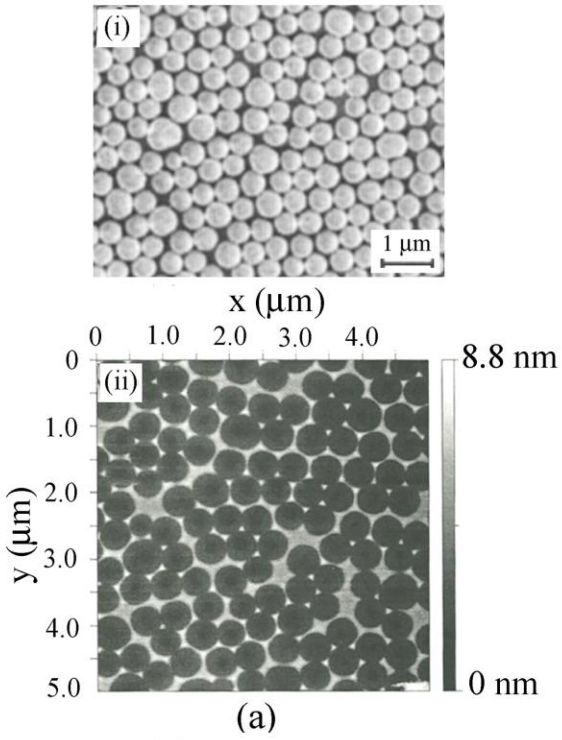

Fig.7.

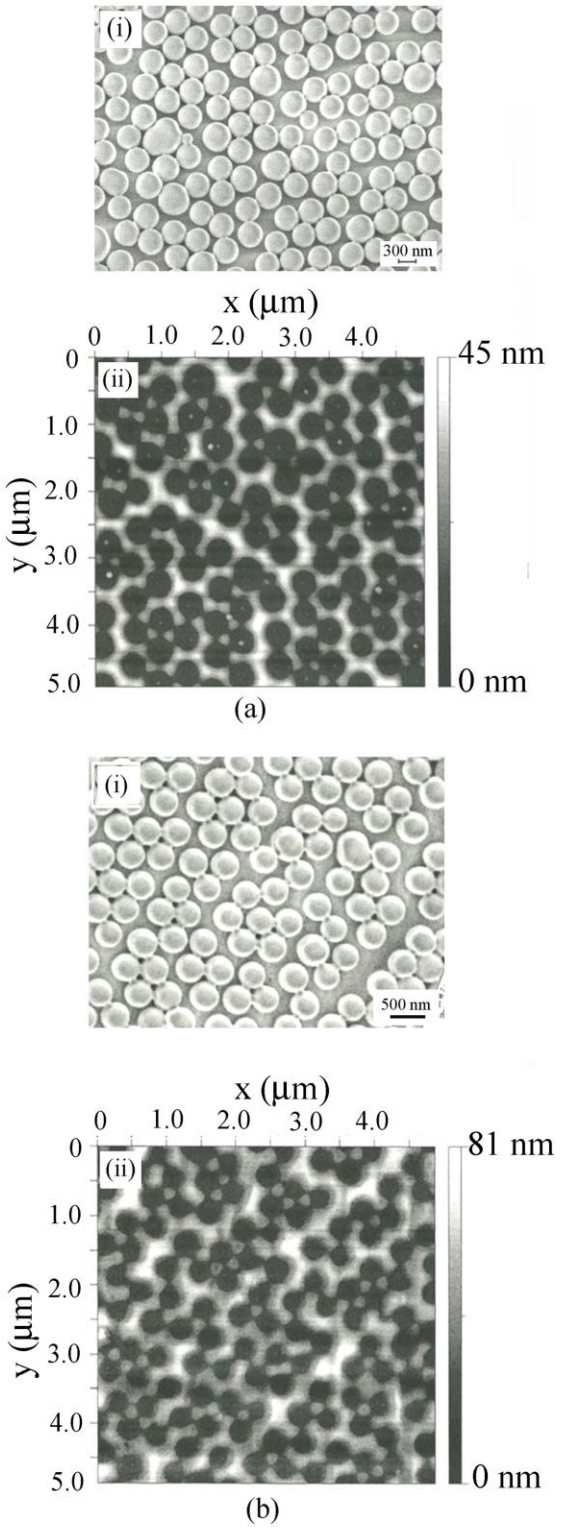

Fig. 8.

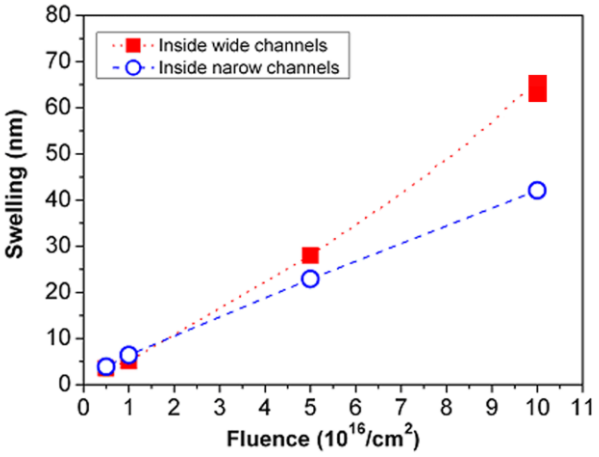

Fig.9.

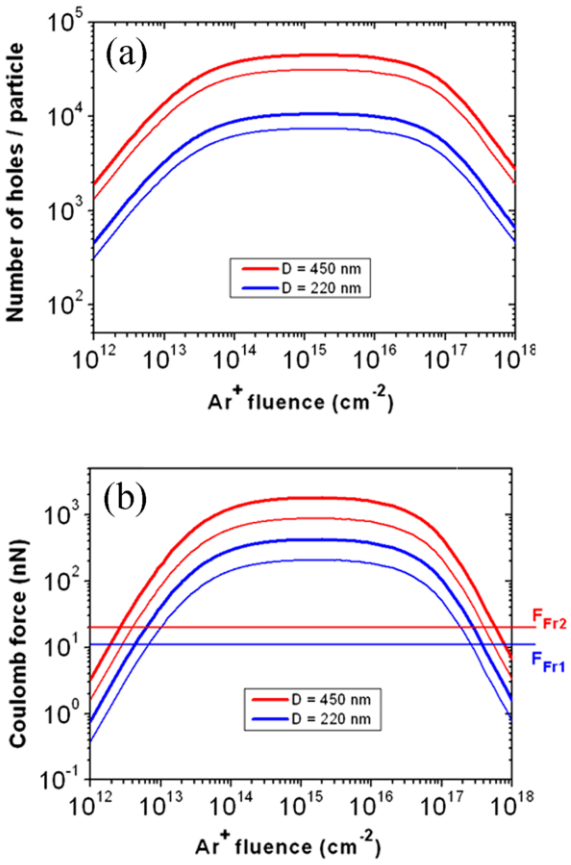

Fig.10.

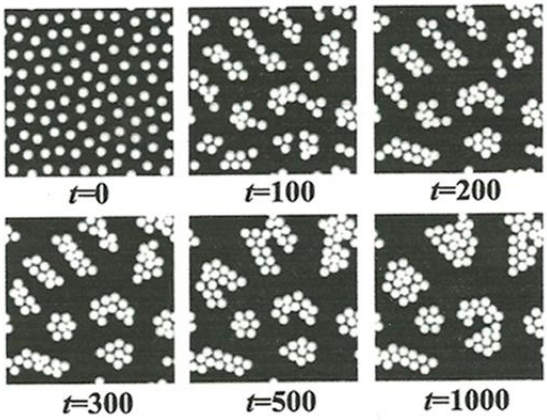

(a)

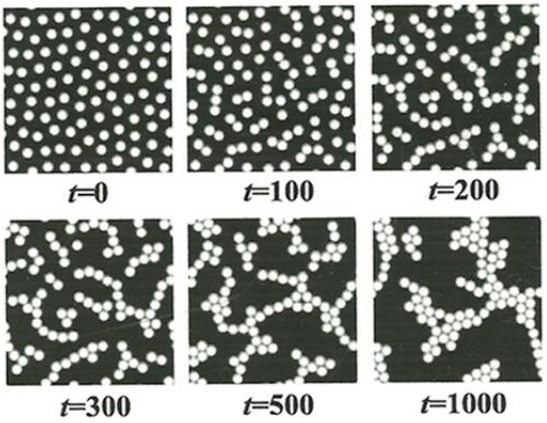

(b)

Fig.11.

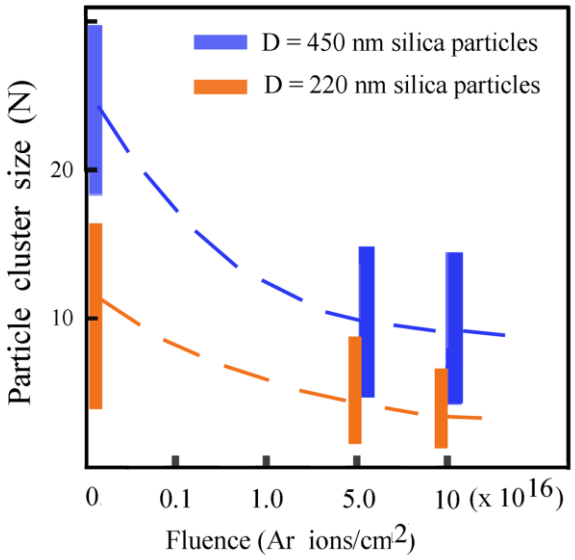

Fig.12.

HIGHLIGHTS

- Reorganization of LB layers under low energy Ar^+ ion irradiation.
- Low fluence: the particles move as solid particles on solid substrate.
- High fluence: the solid particles move on the soft fluid-like substrate.
- Very high fluence: the soft particles move on the soft fluid-like substrate.
- Reorganization is modeled by dynamics of colloidal suspensions.